Heliyon 10 (2024) e30546

Contents lists available at ScienceDirect

Heliyon

journal homepage: www.cell.com/heliyon

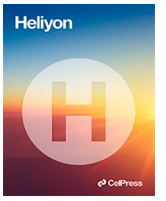

Research article

Synthesis of multi-layer graphene oxide from HCl-treated coke and Brazilian coals by sulfuric acid thermal exfoliation and ozone oxidation

Sergio Nicolas Buitrago Sanchez [a], Julia da Silveira Salla [a], Laura Piacentini Cesconeto [a], Gabriel Lincoln da Rocha [a], Elaine Virmond [b], Regina de Fatima Peralta Muniz Moreira [a,*]

[a] *Department of Chemical Engineering and Food Engineering, Federal University of Santa Catarina, Campus Universitário – Trindade, 88040-900, Florianópolis, SC, Brazil*

[b] *Department of Energy and Sustainability, Federal University of Santa Catarina, Campus Universitário – Araranguá, 88905-120, Araranguá, SC, Brazil*

ARTICLE INFO

Keywords:
Chemical treatment
Oxidative treatment
Sonication

ABSTRACT

This study involved the synthesis and characterization of graphene oxide (GO) from mineral coke and bituminous coal. HCl treated and non-HCl treated ultrafine powder obtained from both precursors were treated with H_2SO_4, followed by thermal treatment, and oxidation with ozone and ultra-sonication for GO production. The synthesized materials were characterized using Fourier transform infrared spectroscopy (FTIR), zeta potential (ZP), particle size distribution (PSD), transmission electron microscopy (TEM), X-ray diffraction (XRD) and Raman spectroscopy. The results confirmed the exfoliation of the material primarily at the edges of its structure and the formation of multilayer graphene oxide (GO) from mineral coke and bituminous coal. Furthermore, it was found that carbonaceous materials with graphitic morphology are easier to exfoliate and oxidize, leading to the production of higher quality graphene oxide. Therefore, the GO synthesized from mineral coke exhibited the best quality in this study. The methodology used proposes an innovative approach, offering a faster, more economical, and environmentally friendly synthesis compared to the traditional Hummers' method, thereby adding value to other raw materials that can be utilized in this process, such as Brazilian coke and coal.

1. Introduction

Mineral coal has recently been proposed for use as a low-cost alternative to graphite as a raw material for graphene production via chemical exfoliation [1–3]. In addition to being low cost, coal is very abundant in several parts of the world. This has led to the development of competitive processes to convert this raw material into a key resource for the manufacture of new materials [4]. Various grades of coal found in abundance are favorable sources for synthesis or for their transformation into nanomaterials such as graphite, graphene oxide, carbon fibers and carbon nanoparticles [5,6].

Graphene-based compounds such as graphene oxide and reduced graphene oxide have received great attention in recent years, and

* Corresponding author.
E-mail address: regina.moreira@ufsc.br (R.F.P.M. Moreira).

https://doi.org/10.1016/j.heliyon.2024.e30546
Received 14 November 2023; Received in revised form 16 April 2024; Accepted 29 April 2024
Available online 30 April 2024

The following abbreviations were used in this manuscript

GO	Graphene Oxide
TEM	Transmission Electron Microscopy
FTIR	Fourier Transform Infrared Spectroscopy
XRD	X-ray Diffraction
ZP	Potential Zeta
PSD	Particle Size Distribution
DLS	Dynamic Light Scattering
ELS	Electrophoretic Light Scattering
AFM	Atomic Force Microscopy
ID/IG	Intensity of the D peak to the intensity of the G peak
La	Crystallite size
U	Moisture
FC	Fixed Carbon
VM	Volatile Material
CZ	Ash
PVDF	polyvinylidene difluoride
Cq	Coke
CB	Mineral Coal B
CS	Mineral Coal S
Cq_OG	Graphene oxide from Coke
Cq_HCl_OG	Graphene oxide from Coke with HCl treatment
CB_OG	Graphene oxide from Mineral Coal B
CB_HCl_OG	Graphene oxide from Mineral Coal B with HCl treatment
CS_OG	Graphene oxide from Mineral Coal S
CS_HCl_OG	Graphene oxide from Mineral Coal B with HCl treatment

due to their excellent electrical, mechanical, and thermal properties have been considered for use in polymer nanocomposites, energy storage, thin films, and degradation of organic pollutants, among other applications [7,8]. Therefore, several methods to produce graphene have been reported, such as electrochemical exfoliation [9–11], arc discharge [12,13], chemical vapor deposition [14], and sonication [15]. The process most used to date is the individual exfoliation of the graphite layers based on the Hummers' method [16–18]. However, some challenges still persist in this procedure, such as the high consumption of oxidants and intercalating agents, which are essential for the quality of the product obtained [19]. The synthesis duration is also lengthy, leading to high production costs on an industrial scale [20]. Additionally, the Hummers' method generates a significant amount of acidic waste, which is challenging to treat and may pose risks to health and the environment [21].

Graphene is not thermodynamically stable due to its melting temperature (3925–3970), which decreases as its thickness decreases. For this reason, a method has been found to go from graphene-to-graphene oxide (GO) [22,23]. GO is composed of functional groups on its surface such as carboxylic acid, hydroxyl, and epoxy. It also has excellent adsorption capacity due to the aromatic hexagonal plane within its structure, which favors strong adhesion to different organic and inorganic molecules [24]. GO can be synthesized by chemical oxidation and exfoliation of graphite. It is also of vital importance to properly introduce reactive functional groups to GO, since this improves the catalytic and adsorption properties for some GO applications. As an example, sulfuric acid (H_2SO_4) is used to oxidize the carbon on the graphite surface, resulting in the formation of functional groups such as carboxyl (-COOH) and hydroxyl (-OH) groups, essential for producing graphene oxide. Likewise, the inclusion of oxygenated groups allows easy dispersion in water and organic solvents [22].

In contrast to the synthesis procedure that have been used, a new method with ozone has been found and it has been shown that ozone gives rise to atomic oxygen and hydroxyl radicals leading to the oxidation of carbon chain, although the mechanism of this reaction is still not clear [25]. According to Lesiak et al. [26], GO was prepared through ozone oxidation, obtaining a lower amount of sp3 carbon atoms and oxygen groups, using a more economical, safe, effective, and environmentally friendly method. Similarly, ozone oxidation and thermal treatment were used to modify the optical properties of GO [27,28].

Nevertheless, the coal-based graphene properties depend on the coal rank, the structural evolution of the coal, degree of graphitization, and ash content [28]. The coal impurities (mineral components) may destroy the integrity of the aromatic layer during graphitization, and the raw coal should be treated by HCl or purified before coal-based graphene preparation [29–31].

The maceral composition of the mineral coals also affects the coal-based graphene properties. Bituminous coal and anthracite are potentially useful for producing graphene, but there is no consensus about the formation mechanisms of coal-based graphene from macerals and the most suitable method for obtaining high yield and optimized properties for each GO application.

Therefore, the main goal of this study was to propose a synthesis procedure to prepare GO from Brazilian coal and coke using chemical and thermal exfoliation and ozone oxidation procedures. This innovative synthesis is more environmentally friendly than traditional synthesis methods. To synthesize a given amount of graphene oxide-based materials, the sulfuric acid consumption using

the Hummers' method is more than 30 times greater than when using the synthesis method proposed in this work, without comparing the quality of the resulting products. Moreover, this method eliminates the use of potassium permanganate ($KMnO_4$) and hydrogen peroxide (H_2O_2) and, in addition, involves the use of in situ ozonation.

2. Materials and methods

Two different Brazilian bituminous coals were supplied by different companies, as designated in Table 1. Additionally, a mineral coke was also used as raw material to prepare GO. Hydrochloric acid (HCl, PA, 37 %, Wt.: 36.458 g mol^{-1}) was purchased from Exôdo Científica (Brazil) and sulfuric acid (H_2SO_4, PA, 99.8 %, Wt.: 98.079 g mol^{-1}) from Vetec (Brazil). Nitrogen under high pressure was purchased from White Martins (Brazil) and ozone was generated in situ by an ozone generator (O3R, Brazil).

The coal samples were treated by adding 500 mL of 20 % hydrochloric acid (HCl) to 10 g of solid coal in a flask under magnetic stirring for 24 h. The suspension was then filtered in a vacuum system using 0.55 μm glass membrane filter followed by washing using deionized water to remove the excess of acid. The samples were dried at 45 °C in oven for 48 h.

Then, the chemical treatment was performed by adding 10 mL of sulfuric acid (H_2SO_4) to the solid and kept in contact for 24 h at room temperature. Thermal exfoliation was performed by placing the mixture in a quartz tubular reactor and left in the furnace at 950 °C for 30 min in an inert nitrogen atmosphere. The furnace was previously heated at a rate of 20 °C min^{-1}. For the oxidative treatment, the resulting powder was suspended in water and treated with ozone for 18 h using a flow rate of 1 L min^{-1}. Next, the aqueous suspension was sonicated in an ultrasonic bath (Unique, model USC-1650A) for 60 min at a frequency of 25 kHz. Finally, the GO was separated by vacuum filtration using 0.22 μm PVDF membrane and oven-dried at 45 °C overnight. Non-HCl treated samples were also submitted to chemical, thermal, oxidation and sonication treatments to examine the effect of the mineral content on the GO properties. Fig. 1 presents a schematic representation of the process applied for obtaining GO.

Table 2 shows the designation given to the synthesized materials according to the treatment applied, where XX can be Cq, CB or CS.

The resulting GO was characterized by X-ray diffraction (XRD) on a Rigaku Miniflex 600 diffractometer operating with radiation CuKα (λ = 0.1542 nm). The X-ray generator was set at a voltage of 40 kV and current of 40 mA. The continuous scan mode was used in a 2θ between 10° and 90° with a step of 0.05° at a rate of 10° min^{-1}. Equation (1), known as the Scherrer equation, was used to determine the crystallite size, where λ is the radiation wavelength, θ is the Bragg angle, L is the apparent particle size, β is the half peak width and K is the Scherrer constant [32].

$$\beta = K\lambda/L.\cos\theta, \tag{1}$$

The zeta potential of the sample was determined by electrophoretic light scattering (ELS) at 173° on a Malvern MPT-2 equipment. The particle size distribution was determined by dynamic light scattering (DLS) on a Malvern Zetasizer Nanosizer (0.3 nm–10 μm). The Fourier transform infrared spectroscopy (FTIR) was analyzed on a PerkinElmer Spectrum 100 equipment, using KBr pellets and a wavenumber range of 4000 to 400 cm^{-1}. The morphology of the resulting material was obtained by transmission electron microscopy (TEM) on a JEM-2100 microscope with a maximum accelerating voltage of 200 kV. The proximate analysis was done in the Shimadzu DTA-60 equipment and the analysis conditions can be seen in Table 3.

3. Results and discussion

3.1. Proximate analysis

For the production of GO, it is important to know the composition and quality of the raw materials used as they can influence the quality of the products obtained. For coal and coke, the content of moisture (U), fixed carbon (FC), volatile matter (VM) and ash (Z) are important information that reveal characteristics of their composition. The moisture content was determined by the difference between the weight of the wet sample (at 25 °C) and the weight of the dry sample (at 100 °C) divided by the weight of the wet sample during the proximate analysis. The parameters in the dry basis were obtained by Equations (2)–(5).

$$U = \frac{(wet\ weight - dry\ weight)}{wet\ weight} x\ 100 \tag{2}$$

$$VM' = VM\frac{100}{100 - U} \tag{3}$$

$$Z' = Z\frac{100}{100 - U} \tag{4}$$

Table 1
Sample names and nomenclature of coke and coal.

Supplier	Sample	Nomenclature
Company B, Brazil	Mineral coke	Cq
Company B, Brazil	Bituminous coal	CB
Company S, Brazil	Bituminous coal	CS

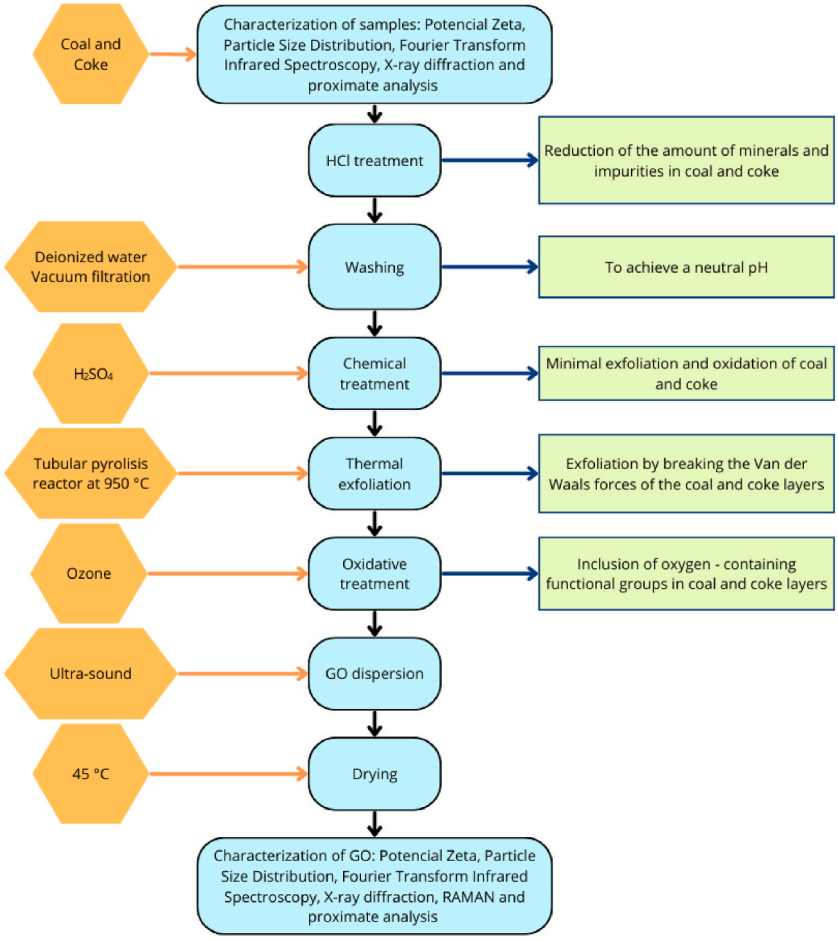

Fig. 1. Schematic process to obtain GO.

Table 2
Nomenclature of the product samples according to the treatment applied.

Nomenclature[a]	Treatment
XX_HCl_OG	HCl treatment, thermal exfoliation followed by oxidation with ozone and sonication
XX_OG	Thermal exfoliation followed by oxidation with ozone and sonication

[a] where XX can be Cq, CB or CS.

Table 3
Conditions applied for proximate analysis.

Temperature rate, °C/min	Holding temperature, °C	Retention time, min	Gas
10	35	20	N_2
50	50	5	N_2
50	110	5	N_2
20	950	15	N_2
−10	750	0	Air
1	750	40	Air

$$FC' = 100\% - MV - CZ \quad (5)$$

The percentage of fixed carbon is the portion of carbon that remains as a residue after the volatile matter has been removed from the material. It usually consists only of carbon, but may contain traces of hydrogen, oxygen, nitrogen and sulfur [33]. Volatile matter is composed of components that burn easily in the presence of oxygen, including short- and long-chain hydrocarbons and aromatics [34,35]. Finally, ash refers to the inorganic residues remaining after the heat treatment of coal. These residues are mainly composed of minerals that do not burn during coal combustion and generally consist of oxides of silicon, aluminum, iron, calcium, magnesium and other elements present in the rocks from which the coal was formed [36].

Table 4 shows that the percentage of VM was considerably reduced in CB and CS samples, with a reduction of 15.29 % and 17.52 %, respectively. On the other hand, there was a small increase in the VM content for coke, which was expected since coke is a material that has been previously treated at a high temperature.

It was expected that the chemical treatment would be able to almost completely reduce the percentage of ashes, which can interfere with subsequent stages of the process. However, Table 4 shows that Cq slightly decreases its ash content (0.68 %) while CB and CS increase this content. This is due to the fact that the coal samples were treated only with HCl, which will eliminate a smaller amount of minerals, as this acid is not capable of eliminating other minerals present in the ash in large quantities, such as SiO_2 [37,38].

Furthermore, some particular cases can be observed, such as coke, which suffered a certain decrease in its fixed carbon content after going through the ozonation process. This may occur because some oxygen atoms present in ozone can bind to carbon atoms from the material and be released in the form of CO or CO_2, even if in small quantities.

3.2. FTIR analysis

The FTIR spectra of the different GO synthesized (Fig. 2) show the presence of absorption bands at 1032 cm^{-1}, 1053 cm^{-1} and 1426 cm^{-1}, which are attributed to C–O stretching vibrations [39,40]. The 1032 cm^{-1} peak is less intense for Cq_OG, while good intensity is seen for Cq_HCl_OG and CS_OG materials. The 1053 cm^{-1} peak is only seen in CB_OG, CB_HCl_OG and CS_OG samples, although in the latter material its intensity is low. Meanwhile, the 1426 cm^{-1} peak is only found in CS_OG sample with medium intensity. The peak at 1529 cm^{-1} is related to C═C stretching [40–42] and is found with a low intensity in Cq_HCl_OG, CB_OG and CB_HCl_OG. A characteristic peak of commercial GO, at 1600 cm^{-1}, is attributed to the O–H vibrations of water [41] and can be found in materials made from coal. Likewise, in materials originating from coke, two high intensity peaks at 2039 cm^{-1} and 2155 cm^{-1} are identified, related to the C═C═C stretching of a material derived from coal. Similarly, in CS_OG, the peaks at 2835 cm^{-1} and 2919 cm^{-1} correspond to the hydrogen bonded in OH groups of the COOH groups and the O–H stretching [41]. In the materials made from CB and CS coals, a large amplitude peak was observed at 3428 cm^{-1} with strong intensity, which corresponds to the stretching vibrations of the OH groups of water [42,43]. Finally, in CS_OG, there were more oxygenated groups because the oxidation with ozone was more effective than in the other GO syntheses. Similarly, it could be noted that the materials made from coke were the poorest in oxygenated groups, although they still presented peaks characteristic of untreated coal.

3.3. Zeta potential analysis

The zeta potential of samples was measured in aqueous solution at neutral pH to determine the stability of the synthesized GOs, which is dependent on the stabilization of the electrostatic charge (Table 5) [44].

The results obtained for all prepared GO had negative values, which may be due to the ionization of the carboxylic acid group and the appearance of negatively charged functional groups [37,45]. Likewise, a high negative value would indicate a high physical stability. Therefore, the carbon-based materials obtained in this study achieved a zeta potential more negative than its initial value, indicating the improvement in the electrical activity and the inhibition of aggregates due to electrostatic repulsion [44]. However, the materials synthesized from coke did not improve their stability, achieving a less negative zeta potential value than the initial coke value.

Table 4
Results of the proximate analysis of the raw and treated samples.

Nomenclature	Fixed Carbon, wt% (db[a])	Volatile Matter, wt% (db)	Ash, wt% (db)
Cq	82.39	6.70	10.91
Cq_OG	77.49	9.00	13.51
Cq_HCl_OG	81.37	8.39	10.23
CB	52.32	33.18	14.50
CB_OG	58.31	23.60	18.09
CB_HCl_OG	63.45	17.89	18.66
CS	54.46	31.26	14.27
CS_OG	68.77	17.39	13.84
CS_HCl_OG	68.42	13.74	17.84

[a] db: dry basis.

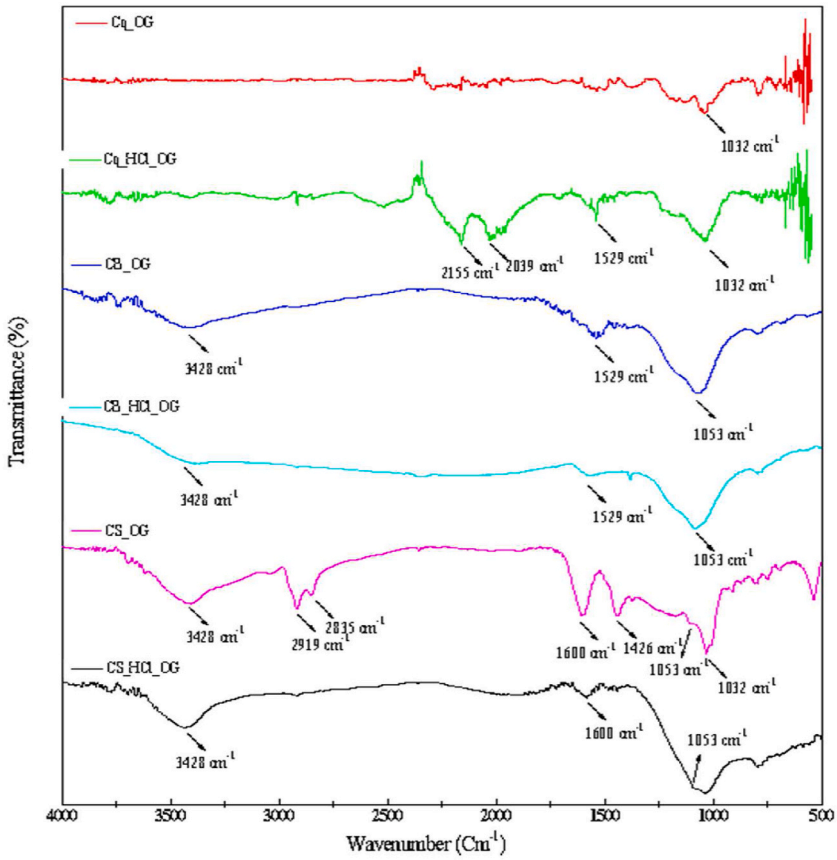

Fig. 2. FTIR spectrum of the treated samples Cq_OG, Cq_HCl_OG, CB_OG, CB_HCl_OG, CS_OG and Cq_HCl_OG.

Table 5
Results for zeta potential for the aqueous dispersions obtained from raw and treated samples.

Nomenclature	Zeta potential, mV
Cq	−26.4
Cq_OG	−21.3
Cq_HCl_OG	−17.8
CB	8.6
CB_OG	−14.1
CB_HCl_OG	−17.5
CS	−14.2
CS_OG	−25.36
CS_HCl_OG	−21.2

3.4. Particle size distribution

Particle size distribution has been reported as a simple and fast method for graphene characterization [46]. Fig. 3 shows the particle size distributions of all the carbon-based materials with a Gaussian approximation. For CS_OG, an average size of 3800 nm was determined, being the largest particle size achieved. The second largest particle size has an average of 1500 nm and is from Cq_OG, while for the rest of the synthesized materials a particle size between 200 nm and 800 nm can be observed.

The initial particle sizes of Cq, CB and CS were 1403 nm, 1306 nm and 3236 nm, respectively. In fact, the particle size of the graphene obtained according to previous studies is related to the size of the coke or coal used [47], which was also observed in this study. For Cq_OG and CS_OG samples, the size remained the same or very similar to the initial size. On the other hand, for Cq_HCl_OG, CB_HCl_OG and CB_OG samples, a reduction in size of 42 %, 38 % and 35 % respectively, was achieved. The material that reduced its size the most was CS_OG, with a reduction of 78.3 %, initially being the largest. Thus, smaller particles can be achieved by breaking down larger carbon particles during synthesis, increasing the hydrophilic property of the obtained graphene-based material [47,48].

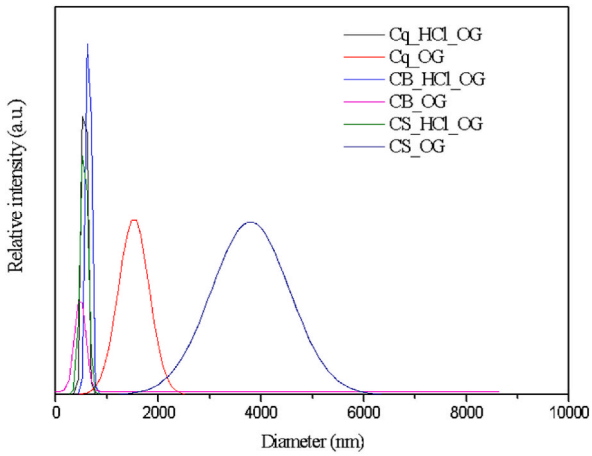

Fig. 3. Results of the DTP analysis for the treated samples Cq_OG, Cq_HCl_OG, CB_OG, CB_HCl_OG, CS_OG and Cq_HCl_OG.

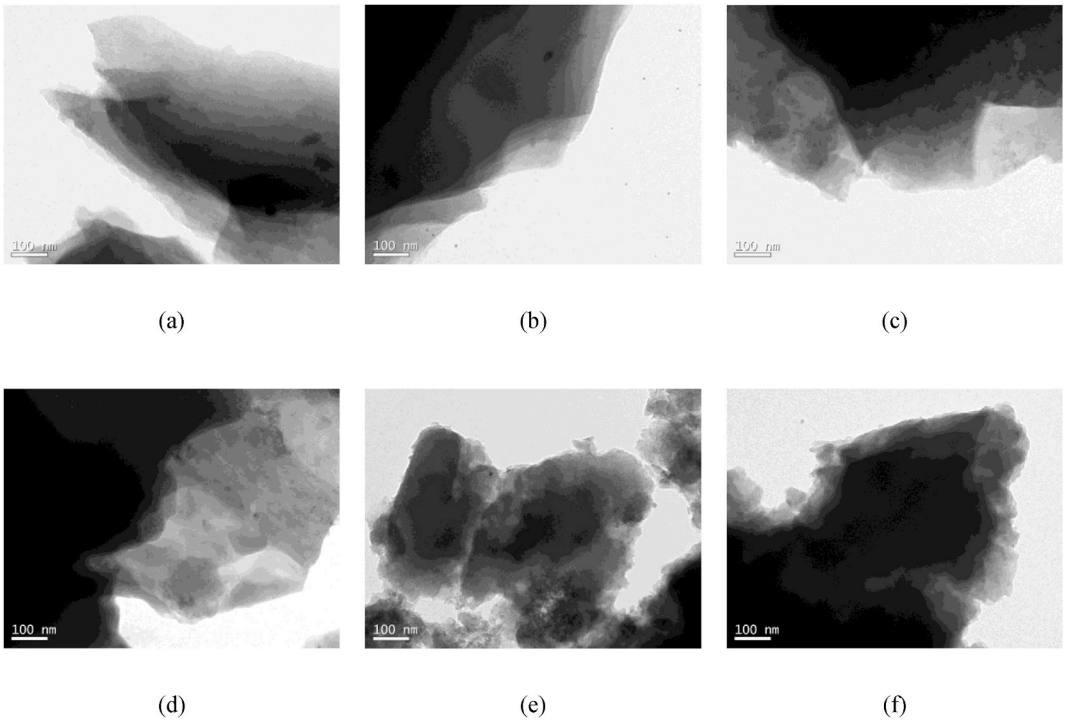

Fig. 4. TEM of the samples (a) Cq_HCl_OG, (b) Cq_OG, (c) CB_HCl_OG, (d) CB_OG, (e) CS_HCl_OG and (f) CS_OG.

3.5. TEM analysis

The morphology of the synthesized GO was studied by TEM images and the results are presented in Fig. 4(a–f).

The morphology for the GOs produced were similar, mostly formed by lamellae with different transparencies, which reveal the nature of the material [49]. In fact, the darker portions correspond to regions where there is greater layer stacking (multilayers), while the more transparent parts are formed by one or two layers [50]. This can occur when exfoliation is not complete throughout the structure, but occurs mainly at the edges of the GO layers. This may happen since coal and coke are not homogeneous or completely ordered materials like graphite. In addition, they are materials that can contain large amounts of impurities. This means that when H_2SO_4 is added, it experiences difficulty placing its atoms in the innermost parts of the material [26–28]., but can do so easily at the edges. Therefore, GOs produced from coke (Fig. 4a and b) or coal (Fig. 4c–f) are not high-purity materials, but they can be used in a variety of applications that do not require a single-layer graphene-based material. Furthermore, after oxidation with ozone, oxygenated functional groups were expected to form at the edges of the materials layers, as was observed in the results obtained by

FTIR (Fig. 2). Likewise, the presence of darker parts in the TEM images (Fig. 4a–f) may indicate a low stability of the GO due to the tendency of the layers to come together again due to the van der Waals attraction force. It may also be due to the adsorption of contaminants on the surface at room temperature, which makes it difficult to directly observe the morphology of GO [51].

3.6. XRD analysis

The results obtained by XRD are presented in Fig. 5(a–c). The graphs show the initial and post-treatment conditions for each sample. For the three raw materials, Cq (Fig. 5a), CB (Fig. 5b) and CS (Fig. 5c), the peak at 26.5° can be identified, which is characteristic of bituminous coal and confirms the presence of quartz. On the other hand, CS presents hematite derived from the reaction between sulfur from pyrite and calcite from coal [52].

The peak at 26.5° was present in all the GOs produced, which means that GO may be mixed with quartz (ICSD-0861560). This peak was lower after the treatments performed in this work, which is characteristic of the formation of GO from carbon exfoliation. A peak at 19.5° is related to kaolinite (ICSD-0291488). Likewise, the incomplete reduction of these peaks indicates that demineralization with HCl was not effective in removing ash content from the raw materials, as also observed in Table 4. The crystal size, shown in Table 6 and determined by Equation (1), decreased after the treatments performed, confirming the expected behavior in the transformation of carbon to GO [40,53–55]. The non-demineralization of carbon can also be seen in Table 6, where the carbon-based materials crystal size were 22.3 nm and 20.2 nm for CB_HCl_OG and CS_HCl_OG, respectively, while the average value expected for a completely demineralized material is 2.354 nm.

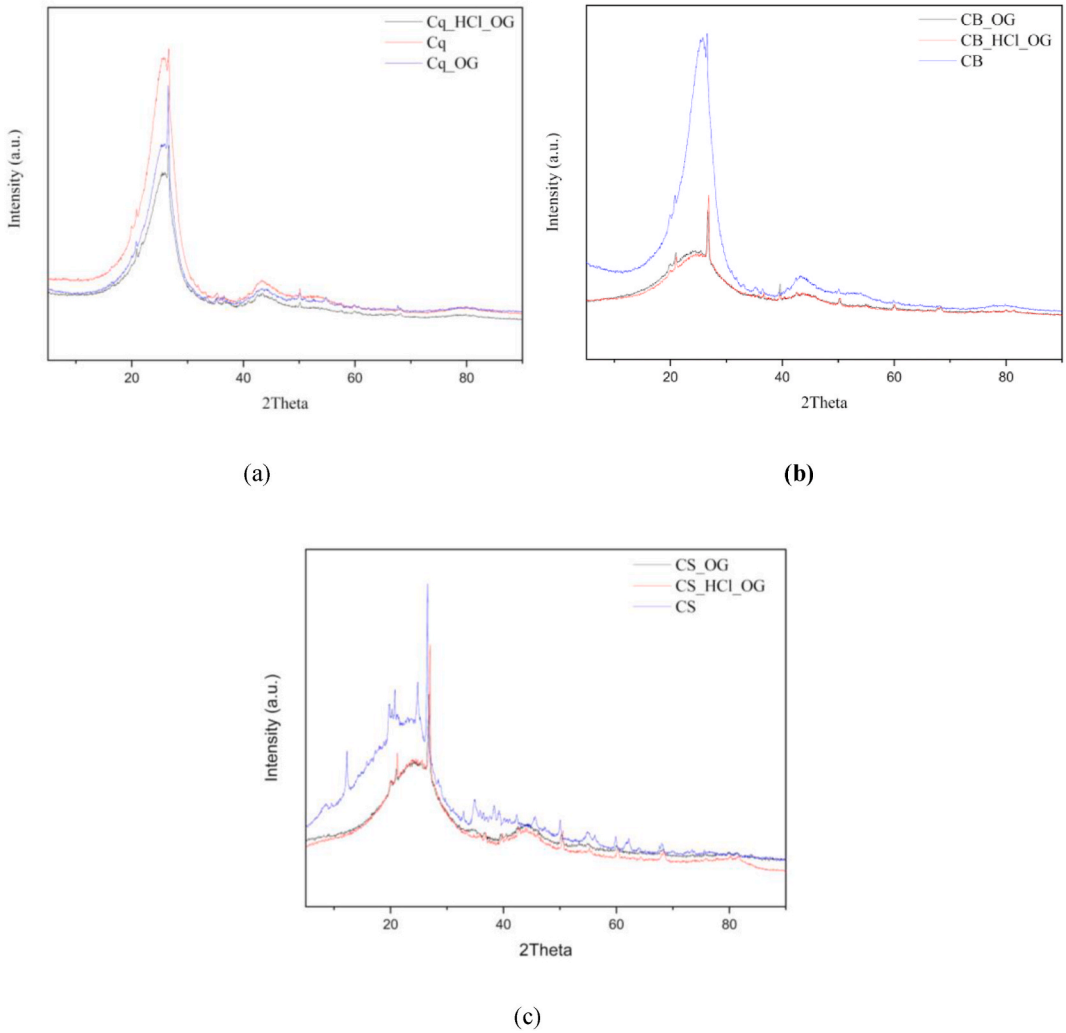

Fig. 5. XRD results obtained for the raw and treated samples (a) Cq, Cq_OG, Cq_HCl_OG, (b) CB, CB_OG, CB_HCl_OG, (c) CS, CS_OG and CS_HCl_OG.

Table 6
Crystal size of the raw and treated samples Cq, Cq_OG, Cq_HCl_OG, CB, CB_OG, CB_HCl_OG, CS, CS_OG and Cq_HCl_OG.

Nomenclature	Crystal size, nm
Cq	3.1
Cq_OG	2.6
Cq_HCl_OG	0.8
CB	25.3
CB_OG	20.9
CB_HCl_OG	22.3
CS	24.2
CS_OG	22.8
CS_HCl_OG	20.2

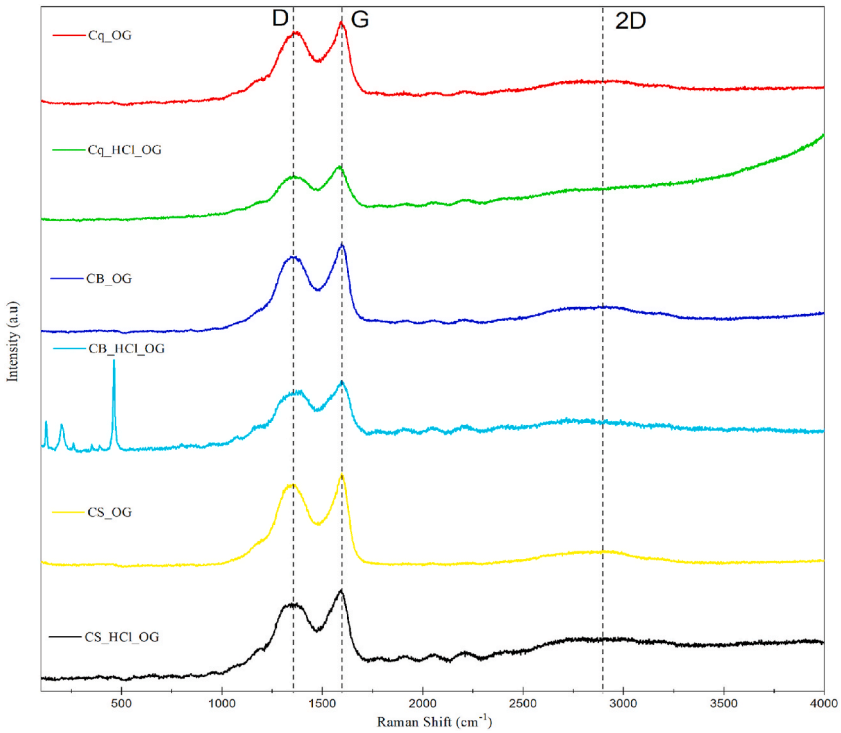

Fig. 6. Raman spectra obtained for the treated samples Cq_OG, Cq_HCl_OG, CB_OG, CB_HCl_OG, CS_OG and CS_HCl_OG.

3.7. Raman analysis

The Raman spectra for GO synthesized samples are shown in Fig. 6. The D-band can be seen at 1376 cm^{-1} and the G-band at 1596 cm^{-1}, which corresponds to the order dispersion of the E2g mode. The 2D-band at 2893 cm^{-1} corresponds to the overtone of the D-band and is helpful for determining the structural parameters of the c-axis orientations [56]. Meanwhile, in the materials synthesized from coke, a D band can be seen with lower intensity than in those produced by coal, which may be due to a defective formation and the presence of hetero-atoms in the plane grain boundaries. Similarly, the intensity of the 2D band was minimal due to the breaking of the stacking of the coal and coke layers by oxidation with sulfuric acid [56].

The bands observed for the treated samples are in agreement with other GOs reported in the literature [51,57–59]. The characterization of GO synthesized through the methods proposed in this study has shown a G band towards a higher wavenumber, which means that GO has a higher oxidation level.

Moreover, the crystallite size (La) of each material can be seen in Table 7 and Equation (6) was used for this calculation. The ID/IG ratio is used to verify whether the material was modified during the synthesis performed. Amaro-Gahete et al. [46] reported an ID/IG ratio for coal of 0.10, similar to the values obtained for Cq, CS and CB, between 0.8 and 0.9, which means that this ratio increased, confirming the exfoliation of coal and coke [49]. The crystallite size of the synthesized materials was calculated according to Equation (6).

Table 7
I_D/I_G ratio values and crystallite size (La) estimated by RAMAN spectroscopy for the GO samples obtained.

Nomenclature	I_D/I_G	La, nm
Cq_OG	0.854	22
Cq_HCl_OG	0.900	21
CB_OG	0.876	22
CB_HCl_OG	0.899	21
CS_OG	0.897	21
CS_HCl_OG	0.887	21

$$La(nm) = \frac{(2.4x10 - 10)(\lambda)^4}{I_D/I_G}, \quad (6)$$

All materials presented similar crystallite size (La), and the results agree with XRD results. From the I_D/I_G ratio, it is possible to conclude that multilayered materials were synthesized by the thermal exfoliation followed by oxidation with ozone and ultrasound.

4. Conclusions

In this study, multilayer GO was synthesized from coke and coal as base materials and was characterized by FTIR, ZP, TEM, XRD and Raman. H_2SO_4 was used as a chemical agent responsible for a prior insertion of oxygenated groups into the structure of the material, mainly at the edges of the material. Furthermore, the combination of H_2SO_4 and high temperature is particularly important in this step, as the heat treatment acts to separate the layers of the material, facilitating the penetration of the sulfuric acid. Subsequently, in situ ozonation proved to be efficient to produce oxidized materials. The sample of GO prepared from mineral coal was the most oxidized of the synthesized materials and this is proven by the amount of oxygenated groups seen in the FTIR spectra and by the decrease of 78.3 % in crystal size. XRD pattern showed a peak at 26° with a lower intensity after the treatments performed. TEM images revealed that the exfoliation of coal- and coke-based materials was better at the edges than in the internal structure of these materials. Graphene oxide synthesized from coke proved to have better quality and better stability than those prepared from mineral coal. The methodology proposed in this study presents a new method of rapid, economical and more environmentally friendly synthesis than the traditional methods used, in addition to diversifying the raw materials used, adding value to mineral coal and coke. Finally, HCl was used as a necessary pretreatment for coal and coke raw materials in order to remove mineral impurities present in this type of material, but it seemed recommendable that future studies investigate demineralization with HF and HCl to reduce the initial percentage of coal ash in order to obtain a higher purity GO.

Funding

This research was funded by FAPESC, Brazil (Grant 2021TR2151 and GRANT 2023TR000324); FEESC (202200081); and Conselho Nacional de Desenvolvimento Científico e Tecnológico - CNPq, Brazil.

Data availability statement

The data that support the findings of this study are available from the corresponding author, R F P M M, upon reasonable request.

CRediT authorship contribution statement

Sergio Nicolas Buitrago Sanchez: Writing – original draft, Methodology, Formal analysis, Data curation, Conceptualization. **Julia da Silveira Salla:** Writing – review & editing, Formal analysis, Conceptualization. **Laura Piacentini Cesconeto:** Investigation, Data curation. **Gabriel Lincoln da Rocha:** Conceptualization. **Elaine Virmond:** Writing – review & editing, Project administration, Funding acquisition, Conceptualization. **Regina de Fatima Peralta Muniz Moreira:** Writing – review & editing, Supervision, Project administration, Funding acquisition, Conceptualization.

Declaration of competing interest

The authors declare the following financial interests/personal relationships which may be considered as potential competing interests:Regina de Fatima Peralta Muniz Moreira reports a relationship with Elsevier B.V. that includes: board membership. If there are other authors, they declare that they have no known competing financial interests or personal relationships that could have appeared to influence the work reported in this paper.

References

[1] V. Purwandari, M. Rianna, Marpongahtun, I. Isnaeni, Y. Zou, M. Harahap, G. Halawa, R. Goei, A.I.Y. Tok, The role of biocatalysts in the synthesis of graphene nanosheets from sub-bituminous coal, Materials Science for Energy Technologies 6 (2023) 282–289, https://doi.org/10.1016/j.mset.2023.02.004.

[2] G. Liu, K. Li, J. Jia, Y. Zhang, Coal-based graphene as a promoter of TiO2 catalytic activity for the photocatalytic degradation of organic dyes, N. Carbon Mater. 37 (2022) 1172–1180, https://doi.org/10.1016/S1872-5805(21)60047-1.

[3] S.-Y. Lee, R.L. Mahajan, A facile method for coal to graphene oxide and its application to a biosensor, Carbon 181 (2021) 408–420, https://doi.org/10.1016/j.carbon.2021.05.007.

[4] S. Vasireddy, B. Morreale, A. Cugini, C. Song, J.J. Spivey, Clean liquid fuels from direct coal liquefaction: chemistry, catalysis, technological status and challenges, Energy Environ. Sci. 4 (2011) 311–345, https://doi.org/10.1039/C0EE00097C.

[5] V.C. Hoang, M. Hassan, V.G. Gomes, Coal derived carbon nanomaterials – recent advances in synthesis and applications, Appl. Mater. Today 12 (2018) 342–358, https://doi.org/10.1016/j.apmt.2018.06.007.

[6] H. Li, X. He, T. Wu, B. Jin, L. Yang, J. Qiu, Synthesis, modification strategies and applications of coal-based carbon materials, Fuel Process. Technol. 230 (2022) 107203, https://doi.org/10.1016/j.fuproc.2022.107203.

[7] P. Sahoo, L. Shubhadarshinee, B.R. Jali, P. Mohapatra, A.K. Barick, Synthesis and characterization of graphene oxide and graphene from coal, Mater. Today: Proc. 56 (2022) 2421–2427, https://doi.org/10.1016/j.matpr.2021.08.206.

[8] D. Smržová, L. Szatmáry, P. Ecorchard, A. Machálková, M. Maříková, P. Salačová, M. Straka, Carbon and zeolite-based composites for radionuclide and heavy metal sorption, Heliyon 8 (12) (2022) e12293.

[9] R. Francisco, Síntesis y caracterización morfológica y electroquímica de puntos cuánticos de grafeno. http://bibdigital.epn.edu.ec/handle/15000/22886, 2022. (Accessed 15 March 2023).

[10] F. Liu, C. Wang, X. Sui, M.A. Riaz, M. Xu, L. Wei, Y. Chen, Synthesis of graphene materials by electrochemical exfoliation: recent progress and future potential, Carbon Energy 1 (2019) 173–199, https://doi.org/10.1002/cey2.14.

[11] P. Yu, S.E. Lowe, G.P. Simon, Y.L. Zhong, Electrochemical exfoliation of graphite and production of functional graphene, Curr. Opin. Colloid Interface Sci. 20 (2015) 329–338, https://doi.org/10.1016/j.cocis.2015.10.007.

[12] Z.-S. Wu, W. Ren, L. Gao, J. Zhao, Z. Chen, B. Liu, D. Tang, B. Yu, C. Jiang, H.-M. Cheng, Synthesis of graphene Sheets with high electrical conductivity and good thermal stability by hydrogen arc discharge exfoliation, ACS Nano 3 (2009) 411–417, https://doi.org/10.1021/nn900020u.

[13] Z. Wang, N. Li, Z. Shi, Z. Gu, Low-cost and large-scale synthesis of graphene nanosheets by arc discharge in air, Nanotechnology 21 (2010) 175602, https://doi.org/10.1088/0957-4484/21/17/175602.

[14] M. Saeed, Y. Alshammari, S.A. Majeed, E. Al-Nasrallah, Chemical Vapour deposition of graphene—synthesis, characterization, and applications: a review, Molecules 25 (2020) 3856, https://doi.org/10.3390/molecules25173856.

[15] A. Kaur, J.A. Morton, A.V. Tyurnina, A. Priyadarshi, A. Holland, J. Mi, K. Porfyrakis, D.G. Eskin, I. Tzanakis, Temperature as a key parameter for graphene sono-exfoliation in water, Ultrason. Sonochem. 90 (2022) 106187, https://doi.org/10.1016/j.ultsonch.2022.106187.

[16] D.C. Marcano, D.V. Kosynkin, J.M. Berlin, A. Sinitskii, Z. Sun, A. Slesarev, L.B. Alemany, W. Lu, J.M. Tour, Improved synthesis of graphene oxide, ACS Nano 4 (2010) 4806–4814, https://doi.org/10.1021/nn1006368.

[17] K. Priyadharshini, S. Rathinavel, E. Velumani, A. Manikandan, Green synthesis and application of graphene oxide extracted from Punica granatum, Mater. Today: Proc. (2023) S2214785323001360, https://doi.org/10.1016/j.matpr.2023.01.085.

[18] E.H. Sujiono, Zurnansyah, D. Zabrian, M.Y. Dahlan, B.D. Amin, J. Agus Samnur, Graphene oxide based coconut shell waste: synthesis by modified Hummers method and characterization, Heliyon 6 (8) (2020) e04568.

[19] H. Yu, B. Zhang, C. Bulin, R. Li, R. Xing, High-efficient synthesis of graphene oxide based on improved Hummers method, Sci. Rep. 6 (2016) 36143, https://doi.org/10.1038/srep36143.

[20] Y. Miao, X. Wang, Y. Liu, Z. Liu, W. Chen, Preparation of graphene oxide/Cellulose composites with Microcrystalline Cellulose acid hydrolysis using the waste acids generated by the Hummers method of graphene oxide synthesis, Polymers 13 (2021) 4453, https://doi.org/10.3390/polym13244453.

[21] C. Powell, G.W. Beall, Graphene oxide and graphene from low grade coal: synthesis, characterization, and applications, Curr. Opin. Colloid Interface Sci. 20 (2015) 362–366, https://doi.org/10.1016/j.cocis.2015.11.003.

[22] O.J. Ajala, J.O. Tijani, M.T. Bankole, A.S. Abdulkareem, A critical review on graphene oxide nanostructured material: properties, Synthesis, characterization and application in water and wastewater treatment, Environ. Nanotechnol. Monit. Manag. 18 (2022) 100673, https://doi.org/10.1016/j.enmm.2022.100673.

[23] E. Ganz, A.B. Ganz, L.M. Yang, M. Dornfeld, The initial stages of melting of graphene between 4000 K and 6000 K, Phys. Chem. Chem. Phys. 19 (2017) 3756–3762, https://doi.org/10.1039/C6CP06940A.

[24] H. Chaudhuri, Y.-S. Yun, Synthesis and environmental applications of graphene oxide/layered double hydroxides and graphene oxide/MXenes: a critical review, Separ. Purif. Technol. 297 (2022) 121518, https://doi.org/10.1016/j.seppur.2022.121518.

[25] S. Groveman, J. Peng, B. Itin, I. Diallo, L.M. Pratt, A. Greer, E.J. Biddinger, S.G. Greenbaum, C.M. Drain, L. Francesconi, M. Vittadello, The role of ozone in the formation and structural evolution of graphene oxide obtained from nanographite, Carbon 122 (2017) 411–421, https://doi.org/10.1016/j.carbon.2017.06.092.

[26] B. Lesiak, L. Stobinski, A. Malolepszy, M. Mazurkiewicz, L. Kövér, J. Tóth, Preparation of graphene oxide and characterization using electron spectroscopy, J. Electron. Spectrosc. Relat. Phenom. 193 (2014) 92–99, https://doi.org/10.1016/j.elspec.2014.03.015.

[27] M.T. Hasan, B.J. Senger, P. Mulford, C. Ryan, H. Doan, Z. Gryczynski, A.V. Naumov, Modifying optical properties of reduced/graphene oxide with controlled ozone and thermal treatment in aqueous suspensions, Nanotechnology 28 (2017) 065705, https://doi.org/10.1088/1361-6528/aa5232.

[28] R. Li, Y. Tang, Q. Che, P. Ma, P. Luo, Z. Lu, M. Dong, Effects of coal rank and macerals on the structure characteristics of coal-based graphene materials from anthracite in qinshui coal-field, Minerals 12 (2022) 588, https://doi.org/10.3390/min12050588.

[29] M.S. Nyathi, C.B. Clifford, H.H. Schobert, Characterization of graphitic materials prepared from different rank Pennsylvania anthracites, Fuel 114 (2013) 244–250, https://doi.org/10.1016/j.fuel.2012.04.003.

[30] C. Lan, Y. Tang, X. Huan, Q. Che, Effects of minerals in anthracite on the formation of coal-based graphene, ChemistrySelect 4 (2019) 5937–5944, https://doi.org/10.1002/slct.201900669.

[31] L. Liu, M. Du, G. Li, J. Fan, Y. Cai, Pyrolysis behavior and product distribution of exinite sub-macerals, J. Anal. Appl. Pyrol. 152 (2020) 104957, https://doi.org/10.1016/j.jaap.2020.104957.

[32] L. Goyeneche, Determinación del tamaño de partícula mediante difracción de rayos X. https://repositorio.unican.es/xmlui/bitstream/handle/10902/15651/Martinez%20Goyeneche%20Lucia.pdf?sequence=1, 2018. (Accessed 28 March 2023).

[33] D.K. Sarkar, Fuels and combustion, in: Thermal Power Plant, Elsevier, 2015, pp. 91–137, https://doi.org/10.1016/B978-0-12-801575-9.00003-2.

[34] R. Kumar, R. Anand, Production of biofuel from biomass downdraft gasification and its applications, in: Advanced Biofuels, Elsevier, 2019, pp. 129–151, https://doi.org/10.1016/B978-0-08-102791-2.00005-2.

[35] J. Bottle, A.R.J. White, Coal analysis, in: The Coal Handbook, Elsevier, 2023, pp. 133–161, https://doi.org/10.1016/B978-0-12-824328-2.00002-9.

[36] K.C. Patra, T.R. Rautray, B.B. Tripathy, P. Nayak, Elemental analysis of coal and coal ASH by PIXE technique, Appl. Radiat. Isot. 70 (2012) 612–616, https://doi.org/10.1016/j.apradiso.2011.12.013.

[37] B. Das, R. Kundu, S. Chakravarty, Preparation and characterization of graphene oxide from coal, Mater. Chem. Phys. 290 (2022) 126597, https://doi.org/10.1016/j.matchemphys.2022.126597.

[38] B. Manoj, A.G. Kunjomana, Systematic investigations of graphene layers in sub-bituminous coal, Russ. J. Appl. Chem. 87 (2014) 1726–1733, https://doi.org/10.1134/S1070427214110251.

[39] S. Chaiyakun Rattana, N. Witit-anun, N. Nuntawong, P. Chindaudom, S. Oaew, C. Kedkeaw, P. Limsuwan, Preparation and characterization of graphene oxide nanosheets, Procedia Eng. 32 (2012) 759–764, https://doi.org/10.1016/j.proeng.2012.02.009.

[40] G. Surekha, K.V. Krishnaiah, N. Ravi, R.P. Suvarna, FTIR, Raman and XRD analysis of graphene oxide films prepared by modified Hummers method, J. Phys.: Conf. Ser. 1495 (2020) 012012, https://doi.org/10.1088/1742-6596/1495/1/012012.
[41] C.H. Manoratne, S.R.D. Rosa, I.R.M. Kottegoda, Xrd-Hta, U.V. Visible, FTIR and SEM interpretation of reduced graphene oxide synthesized from high purity vein graphite, Mat Sci Res India 14 (2017) 19–30, https://doi.org/10.13005/msri/140104.
[42] N. Sharma, V. Sharma, Y. Jain, M. Kumari, R. Gupta, S.K. Sharma, K. Sachdev, Synthesis and characterization of graphene oxide (GO) and reduced graphene oxide (rGO) for gas sensing application, Macromol. Symp. 376 (2017) 1700006, https://doi.org/10.1002/masy.201700006.
[43] L. Shahriary, A.A. Athawale, Graphene oxide synthesized by using modified Hummers approach, BRCORP 2 (2014) 58–63.
[44] P. Mahato, S. Choudhuri, C. Kumar, S. Roy, P. Patra, Evaluation of crystal size present in graphene oxide quantum dots using optical and Raman spectroscopy, Mater. Today: Proc. (2022) S221478532206905X, https://doi.org/10.1016/j.matpr.2022.11.066.
[45] F. Han, J. Mao, S. Liu, Preparation of reduced graphene oxide-carbon nanotubes membranes for conductive heating membrane distillation treatment of humic acid, Separ. Purif. Technol. 302 (2022) 122181, https://doi.org/10.1016/j.seppur.2022.122181.
[46] J. Amaro-Gahete, A. Benítez, R. Otero, D. Esquivel, C. Jiménez-Sanchidrián, J. Morales, A. Caballero, F.J. Romero-Salguero, A comparative study of particle size distribution of graphene nanosheets synthesized by an ultrasound-assisted method, Nanomaterials 9 (2019) 152, https://doi.org/10.3390/nano9020152.
[47] M. Huskić, S. Bolka, A. Vesel, M. Mozetič, A. Anžlovar, A. Vizintin, E. Žagar, One-step surface modification of graphene oxide and influence of its particle size on the properties of graphene oxide/epoxy resin nanocomposites, Eur. Polym. J. 101 (2018) 211–217, https://doi.org/10.1016/j.eurpolymj.2018.02.036.
[48] X. Hu, Y. Yu, W. Hou, J. Zhou, L. Song, Effects of particle size and pH value on the hydrophilicity of graphene oxide, Appl. Surf. Sci. 273 (2013) 118–121, https://doi.org/10.1016/j.apsusc.2013.01.201.
[49] H. Feng, R. Cheng, X. Zhao, X. Duan, J. Li, Correction: corrigendum: A low-temperature method to produce highly reduced graphene oxide, Nat. Commun. 4 (2013) 1927, https://doi.org/10.1038/ncomms2848.
[50] L. Stobinski, B. Lesiak, A. Malolepszy, M. Mazurkiewicz, B. Mierwa, J. Zemek, P. Jiricek, I. Bieloshapka, Graphene oxide and reduced graphene oxide studied by the XRD, TEM and electron spectroscopy methods, J. Electron. Spectrosc. Relat. Phenom. 195 (2014) 145–154, https://doi.org/10.1016/j.elspec.2014.07.003.
[51] S.H. Dave, C. Gong, A.W. Robertson, J.H. Warner, J.C. Grossman, Chemistry and structure of graphene oxide via direct imaging, ACS Nano 10 (2016) 7515–7522, https://doi.org/10.1021/acsnano.6b02391.
[52] N.F. Mohamad, A.R. Hidayu, A.A. Sherif, A.S.A.K. Sharifah, Characteristics of bituminous coal, sub-bituminous coal and bottom ash from a coal-fired power plant, in: 2013 IEEE Busi-Ness Engineering and Industrial Applications Colloquium (BEIAC), IEEE, Langkawi, Malaysia, 2013, pp. 571–573, https://doi.org/10.1109/BEIAC.2013.6560193.
[53] S. Hazim, S. Jassim, A.S. Mahmood, M.A. Hamad, A.R. Mahmood, E.M. Ali, M.A. Alheety, Graphene oxide-gastrointestinal drugs for no side effect: ultrasound synthesis and characterization, Mater. Today: Proc. (2023) S2214785322076374, https://doi.org/10.1016/j.matpr.2022.12.265.
[54] S. Saxena, T.A. Tyson, S. Shukla, E. Negusse, H. Chen, J. Bai, Investigation of structural and electronic properties of graphene oxide, Appl. Phys. Lett. 99 (2011) 013104, https://doi.org/10.1063/1.3607305.
[55] V. Gupta, N. Sharma, U. Singh, M. Arif, A. Singh, Higher oxidation level in graphene oxide, Optik 143 (2017) 115–124, https://doi.org/10.1016/j.ijleo.2017.05.100.
[56] K. Krishnamoorthy, M. Veerapandian, K. Yun, S.-J. Kim, The chemical and structural analysis of graphene oxide with different degrees of oxidation, Carbon 53 (2013) 38–49, https://doi.org/10.1016/j.carbon.2012.10.013.
[57] X. Díez-Betriu, S. Álvarez-García, C. Botas, P. Álvarez, J. Sánchez-Marcos, C. Prieto, R. Menéndez, A. de Andrés, Raman spectroscopy for the study of reduction mechanisms and optimization of conductivity in graphene oxide thin films, J. Mater. Chem. C 41 (2013) 6905, https://doi.org/10.1039/c3tc31124d.
[58] J.S. Mehta, A.C. Faucett, A. Sharma, J.M. Mativetsky, How reliable are Raman spectroscopy measurements of graphene oxide? J. Phys. Chem. C 121 (2017) 16584–16591, https://doi.org/10.1021/acs.jpcc.7b04517.
[59] Q. Xu, X. Lin, L. Gan, G. Owens, Z. Chen, Green reduction of graphene oxide using Bacillus sphaericus, J. Colloid Interface Sci. 605 (2022) 881–887, https://doi.org/10.1016/j.jcis.2021.07.102.